Removal of accidental degeneracy in semiconductor quantum dots

Sathwik Bharadwaj,[1] Siddhant Pandey,[1] and L. R. Ram-Mohan[2,*]
[1]*Department of Physics, Worcester Polytechnic Institute, Worcester, Massachusetts 01609, USA*
[2]*Departments of Physics, Electrical and Computer Engineering, and Mechanical Engineering, Worcester Polytechnic Institute, Worcester, Massachusetts 01609, USA*
(Received 25 September 2017; published 20 November 2017)

We present a quantitative analysis of the energy levels and wave functions of carriers in a cubic quantum dot of GaAs embedded in $Ga_{(1-x)}Al_xAs$ with finite confining potential barriers at their interfaces. The energy spectrum has substantially reduced degeneracies compared to the analytically determined energy levels of the infinite-barrier quantum box of the same dimensions. The level degeneracy of states has been explained by group representations of the point group O_h. Projection operators for the irreducible representations provide a way to obtain the linear combinations of the degenerate wave functions which form a basis set for the representations. Energy-level splittings in the presence of externally applied electric and magnetic fields are also studied.

DOI: 10.1103/PhysRevB.96.195305

I. INTRODUCTION

In quantum mechanical systems, degeneracy in the energy spectrum arises from symmetries of the system that are either based on geometry or are internal symmetries. A classic example of such degeneracy is given by the hydrogen atom with its Coulomb potential $-e^2/(4\pi\epsilon_0 r)$ that binds the electron to the proton. Here, $-e$ is the electron charge and ϵ_0 is the permittivity of free space. The spherical rotational symmetry [O(3)] of the Coulomb potential leads to a degeneracy of states of the order of $(2\ell+1)$, where ℓ is the orbital angular momentum quantum number. The surprise from spectroscopic observations was that for a given principal quantum number n, the different allowed orbital angular momentum states for $\ell = 0,1,\ldots,n-1$ all have the same energy [1]. This additional degeneracy, referred to as "accidental degeneracy," was explained by Pauli [2] by identifying a new conserved vector, the Runge-Lenz vector. Fock [3] showed that the hydrogen atom has a symmetry higher than the three-dimensional (3D) rotational symmetry, namely, O(4). This beautiful application of group theory to the degeneracies of a physical system allows us to appreciate the fundamental role of symmetries and hidden symmetries in the quantum mechanics of a physical system. Further developments by Barut and Kleinert [4] showed that the dynamical symmetry group O(4,2) for the hydrogen atom permits the algebraic evaluation of transition matrix elements and provides a complete realization of the dynamics of this problem in algebraic terms.

As early as 1990, Shertzer and Ram-Mohan [5] observed that semiconductor quantum wires with a square cross section exhibit the reduction of degeneracy associated with the infinite square well potential. An electron in a GaAs quantum wire embedded in $Ga_{(1-x)}Al_xAs$ is confined in the transverse direction by a "kitchen-sink" potential due to the finite band offsets in the semiconductor heterostructure. Only some of the doubly degenerate states labeled by the quantum numbers (n_x,n_y) and their permuted partner (n_y,n_x) associated with the infinite well are split in energy when the well height is made finite. The two dimensional (2D) potential well has C_{4v} symmetry. Seven years after our work was reported, the infinite potential well was shown to have an additional symmetry corresponding to the semidirect product of C_{4v} and a 1D continuous group of transformations generated by the dynamical operator $(\partial_x^2 - \partial_y^2)$, which commutes with the Hamiltonian [6].

This example of accidental degeneracy and its removal provides a textbook example of the interplay between group theory and particle dynamics. We can anticipate that the level degeneracy in the 3D infinite well given by the permutations of (n_x,n_y,n_z) will be richer, since the Pythagorean constraint $E \propto n_x^2 + n_y^2 + n_z^2$ can be satisfied in many more ways. The electron's energy $E = (\hbar^2\pi^2/2m^*L^2)(n_x^2 + n_y^2 + n_z^2)$ corresponds to the spherical surface of constant E over the positive octant defined in the number index space, and the degeneracy corresponds to the number of states that fall on such a surface [7]. The larger the energy, the larger is the level degeneracy [7]. Within the range of energies that we have explored, we have observed degeneracies of ~3000. The reduction in this degeneracy for the cubic finite 3D potential well was already anticipated [5].

In this paper, the phenomenon of accidental degeneracy and its reduction for a physical system with point-group symmetry is presented for a GaAs cubic quantum dot embedded in GaAlAs. We note that the spatial confinement of charge carriers in semiconductor quantum dots (QDs) has led to several interesting electronic, optical, and transport properties in such systems [8–10].

Here, we numerically obtain the energy levels of electrons and holes in cubic quantum dots (QDs) of GaAs in $Ga_{(1-x)}Al_xAs$. This is a prototypical system and our methods apply to any of the II-VI or III-V semiconductor material pairs with type-I interfaces.

Almost all previous studies reported in the literature assume that the confining potential is infinite. Shertzer and Ram-Mohan have shown that for heterostructure quantum wires, the infinite-barrier approximation is not valid and, more importantly, the confining potential is not separable. Here we find that the findings from 2D carry over to 3D: for cubic QDs, the energy levels for the finite potential are significantly lower than those obtained with the infinite barrier. More conspicuous is the

*Corresponding author: lrram@wpi.edu

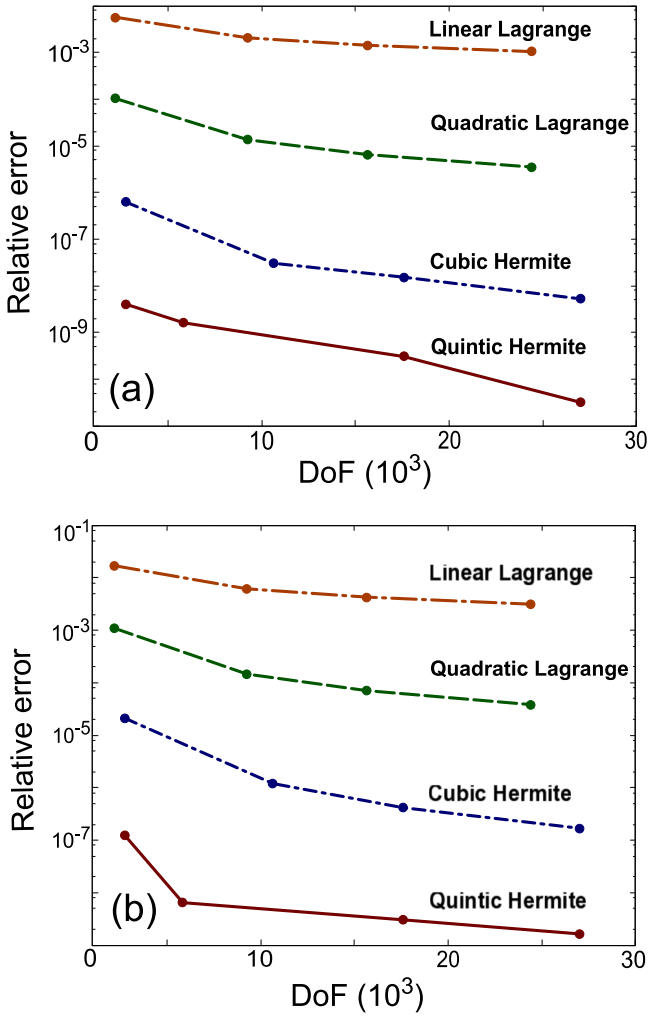

FIG. 1. The convergence of the relative errors in eigenvalues of (a) the ground and (b) the first excited state in the QD for linear Lagrange, quadratic Lagrange, cubic Hermite, and quintic Hermite interpolation polynomials are shown for the case of an infinite quantum well of dimensions 200×200×200 Å. By using quintic Hermite interpolation polynomials, we can reduce the error to 10^{-8} with just 27 elements and 2744 degrees of freedom (DoF), with further reduction in error possible with mesh refinement. The total DoF corresponds to the global matrix dimension.

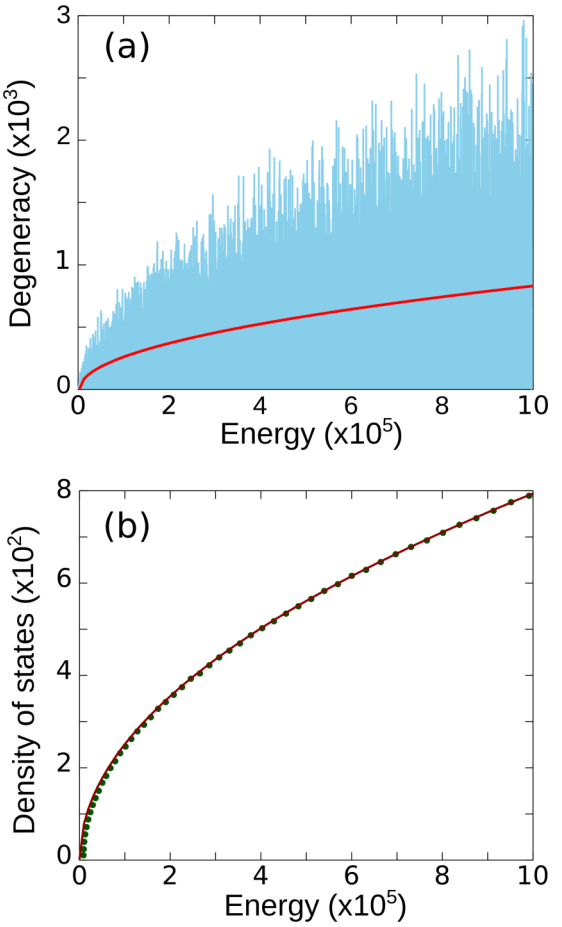

FIG. 2. (a) A histogram for the degree of degeneracy as a function of energy for an infinite-barrier cubic quantum dot. Note that the degeneracy increases without limit, with the largest value shown being ∼3000 in the plot. As the radius of the constant energy surface increases by 1 unit, the level degeneracy fluctuates considerably. The red curve shows the degeneracy averaged over small bins. (b) The calculated density of states (dots) is plotted along with the continuum approximation (continuous curve) of the density of states obtained as the local *average* of the density of states. We see that this evaluation overestimates the density for the lowest of energies, but is found to be an excellent approximation already for intermediate energies. Here the energy is in units of $\hbar^2\pi^2/2m^*L^2 = 0.01413653$ eV. This corresponds to a conduction band electron in a $L = 200$ Å cubic quantum dot.

lifting of the degeneracy of certain energy levels in the energy spectrum of cubic QDs when a finite-well potential is used.

In Sec. II, we use finite-element analysis (FEA) to solve the Schrödinger's equation in the effective-mass approximation. Here, the emphasis is on getting high accuracy in the eigenvalues and eigenfunctions. We show that the use of Hermite interpolation polynomials delivers this; the interface boundary conditions with the additional derivative degrees of freedom (DoF) in the Hermite interpolation can lead to serious bookkeeping issues while implementing jump conditions for the derivatives of wave functions. This is readily overcome by making the use of Fermi-function smoothing, described later in this section. In Sec. III, we use group-representation theory to predict which of the accidental degeneracies present in the infinite cubic well are lifted when a finite barrier is used. In Sec. IV, we discuss results obtained through FEA and investigate splitting of energy levels in the presence of an external electric and magnetic field. With the level of accuracy delivered for actual physical structures discussed here, we mention further directions for research in the concluding remarks of Sec. V. As a final note, FEA transcends geometrical constraints rather cleanly, so that eventually QDs of any shape may be considered for further applications.

II. FINITE-ELEMENT ANALYSIS OF CUBIC QDS

In the envelope-function approximation [11] (EFA), the charge carrier's envelope function $\psi(x,y,z)$ satisfies Schrödinger's equation with a nonseparable potential $V(x,y,z)$

TABLE I. Possible degree of degeneracies due to the permutation of quantum numbers in cubic QDs with infinite-barrier approximation. The level degeneracy can be substantial for large energies, corresponding to the number of ways the Pythagorean sum $(n_x^2+n_y^2+n_z^2)$ corresponds to the given energy. The level degeneracy has no limit and increases with energy. We see in the table that the degrees of degeneracy are already not in accord with the geometrical symmetry group O_h in the low-energy states.

Degree of degeneracy	Example
1	(1,1,1)
3	(1,2,2), (2,1,2), (2,2,1)
6	(1,2,3), (3,1,2), (2,3,1), (2,1,3), (3,2,1), (1,3,2)

corresponding to a finite barrier height,

$$\left[-\nabla\left(\frac{\hbar^2}{2m^*}\nabla\right)+V(x,y,z)\right]\psi(x,y,z)=E\psi(x,y,z), \quad (1)$$

where m^* is the carrier effective mass m_w^* or m_b^* in the quantum dot or the surrounding bulk barrier medium, respectively. The potential is

$$V(x,y,z)=\begin{cases}0 & \text{for } |x|\leqslant a/2,\ |y|\leqslant b/2,\ |z|\leqslant c/2,\\ V_0 & \text{outside.}\end{cases} \quad (2)$$

There is a discontinuity in the potential and the effective mass of the charged carriers at the interface between materials. The continuity of the probability current requires that the wave function $\psi(x)$ and the "mass derivative" of the wave function $(1/m^*)\psi'(x)$ be continuous, as was shown by Ben-Daniels and Duke [12]. The input parameters for the effective masses and band offsets of conduction electrons, heavy holes, and light holes in GaAs and in $Ga_{(1-x)}Al_xAs$ are obtained from Ref. [13]. The FEA employing the action integral formulation [14] is used to evaluate the energies and eigenfunctions. FEA is a generalized variational approach in which we divide the physical domain of interest into several small elements. Within each element, we express the envelope function as a linear combination of interpolation polynomials multiplied by as-yet undetermined coefficients that correspond to the value of the wave function at the vertices (nodes) of the elements that are usually tetrahedra or cubes in 3D. We use

TABLE II. Different possible even and odd combinations of quantum numbers and their corresponding irreducible representations for the symmetry group O_h.

Quantum number	Irreducible representation	Basis function
$(2n-1,2n-1,2n-1)$	$1A_{1g}$	$\psi_{(2n-1,2n-1,2n-1)}$
$(2n,2n,2n)$	$1A_{2u}$	$\psi_{(2n,2n,2n)}$
$(2n-1,2n-1,2m)$	$1T_{1u}$	$\psi_{(2n-1,2n-1,2m)}, \psi_{(2n-1,2m,2n-1)}, \psi_{(2m,2n-1,2n-1)}$
$(2n,2n,2m-1)$	$1T_{2g}$	$\psi_{(2n,2n,2m-1)}, \psi_{(2n,2m-1,2n)}, \psi_{(2m-1,2n,2n)}$
$(2m-1,2n-1,2n-1)$	$1A_{1g}$	$\frac{1}{\sqrt{3}}(\psi_{(2n-1,2n-1,2m-1)}+\psi_{(2n-1,2m-1,2n-1)}+\psi_{(2m-1,2n-1,2n-1)})$
	$1E_g$	$\frac{1}{\sqrt{6}}(-\psi_{(2n-1,2n-1,2m-1)}+2\psi_{(2n-1,2m-1,2n-1)}-\psi_{(2m-1,2n-1,2n-1)})$, $\frac{1}{\sqrt{6}}(2\psi_{(2n-1,2n-1,2m-1)}-\psi_{(2n-1,2m-1,2n-1)}-\psi_{(2m-1,2n-1,2n-1)})$
$(2m,2m,2n)$	$1A_{2u}$	$\frac{1}{\sqrt{3}}(\psi_{(2n,2n,2m)}+\psi_{(2n,2m,2n)}+\psi_{(2m,2n,2n)})$
	$1E_u$	$\frac{1}{\sqrt{6}}(-\psi_{(2n,2n,2m)}+2\psi_{(2n,2m,2n)}-\psi_{(2m,2n,2n)})$, $\frac{1}{\sqrt{6}}(2\psi_{(2n,2n,2m)}-\psi_{(2n,2m,2n)}-\psi_{(2m,2n,2n)})$
$(2n-1,2m-1,2k)$	$1T_{1u}$	$\frac{1}{\sqrt{2}}(\psi_{(2k,2m-1,2n-1)}+\psi_{(2k,2n-1,2m-1)})$, $\frac{1}{\sqrt{2}}(\psi_{(2m-1,2k,2n-1)}+\psi_{(2n-1,2k,2m-1)})$, $\frac{1}{\sqrt{2}}(\psi_{(2m-1,2n-1,2k)}+\psi_{(2n-1,2m-1,2k)})$
	$1T_{2u}$	$\frac{1}{\sqrt{2}}(\psi_{(2k,2m-1,2n-1)}-\psi_{(2k,2n-1,2m-1)})$, $\frac{1}{\sqrt{2}}(\psi_{(2m-1,2k,2n-1)}-\psi_{(2n-1,2k,2m-1)})$, $\frac{1}{\sqrt{2}}(\psi_{(2m-1,2n-1,2k)}-\psi_{(2n-1,2m-1,2k)})$

TABLE III. (Continued from Table II). Different possible even and odd combinations of quantum numbers and their corresponding irreducible representations for the symmetry group O_h.

Quantum number	Irreducible representation	Basis function
$(2n,2m,2k-1)$	$1T_{1g}$	$\frac{1}{\sqrt{2}}(\psi_{(2k-1,2m,2n)}+\psi_{(2k-1,2n,2m)})$, $\frac{1}{\sqrt{2}}(\psi_{(2m,2k-1,2n)}+\psi_{(2n,2k-1,2m)})$, $\frac{1}{\sqrt{2}}(\psi_{(2m,2n,2k-1)}+\psi_{(2n,2m,2k-1)})$
	$1T_{2g}$	$\frac{1}{\sqrt{2}}(\psi_{(2k-1,2m,2n)}-\psi_{(2k-1,2n,2m)})$, $\frac{1}{\sqrt{2}}(\psi_{(2m,2k-1,2n)}-\psi_{(2n,2k-1,2m)})$, $\frac{1}{\sqrt{2}}(\psi_{(2m,2n,2k-1)}-\psi_{(2n,2m,2k-1)})$
$(2m,2n,2k)$	$1A_{1u}$	$\frac{1}{\sqrt{6}}(\psi_{(2m,2n,2k)}-\psi_{(2m,2k,2n)}+\psi_{(2n,2k,2m)}$ $-\psi_{(2n,2m,2k)}+\psi_{(2k,2m,2n)}-\psi_{(2k,2n,2m)})$
	$1A_{2u}$	$\frac{1}{\sqrt{6}}(\psi_{(2m,2n,2k)}+\psi_{(2m,2k,2n)}+\psi_{(2n,2k,2m)}$ $+\psi_{(2n,2m,2k)}+\psi_{(2k,2m,2n)}+\psi_{(2k,2n,2m)})$
	$2E_u$	$\frac{1}{\sqrt{6}}(2\psi_{(2m,2n,2k)}-\psi_{(2n,2k,2m)}-\psi_{(2k,2m,2n)})$, $\frac{1}{\sqrt{6}}(2\psi_{(2n,2k,2m)}-\psi_{(2k,2m,2n)}-\psi_{(2m,2n,2k)})$ $\frac{1}{\sqrt{6}}(2\psi_{(2m,2k,2n)}-\psi_{(2k,2n,2m)}-\psi_{(2n,2m,2k)})$, $\frac{1}{\sqrt{6}}(2\psi_{(2n,2m,2k)}-\psi_{(2m,2k,2n)}-\psi_{(2k,2n,2m)})$
$(2m-1,2n-1,2k-1)$	$1A_{1g}$	$\frac{1}{\sqrt{6}}(\psi_{(2m-1,2n-1,2k-1)}-\psi_{(2m-1,2k-1,2n-1)}+\psi_{(2n-1,2k-1,2m-1)}$ $-\psi_{(2n-1,2m-1,2k-1)}+\psi_{(2k-1,2m-1,2n-1)}-\psi_{(2k-1,2n-1,2m-1)})$
	$1A_{2g}$	$\frac{1}{\sqrt{6}}(\psi_{(2m-1,2n-1,2k-1)}+\psi_{(2m-1,2k-1,2n-1)}+\psi_{(2n-1,2k-1,2m-1)}$ $+\psi_{(2n-1,2m-1,2k-1)}+\psi_{(2k-1,2m-1,2n-1)}+\psi_{(2k-1,2n-1,2m-1)})$
	$2E_g$	$\frac{1}{\sqrt{6}}(2\psi_{(2m-1,2n-1,2k-1)}-\psi_{(2n-1,2k-1,2m-1)}-\psi_{(2k-1,2m-1,2n-1)})$, $\frac{1}{\sqrt{6}}(2\psi_{(2n-1,2k-1,2m-1)}-\psi_{(2k-1,2m-1,2n-1)}-\psi_{(2m-1,2n-1,2k-1)})$
		$\frac{1}{\sqrt{6}}(2\psi_{(2m-1,2k-1,2n-1)}-\psi_{(2k-1,2n-1,2m-1)}-\psi_{(2n-1,2m-1,2k-1)})$, $\frac{1}{\sqrt{6}}(2\psi_{(2n-1,2m-1,2k-1)}-\psi_{(2m-1,2k-1,2n-1)}-\psi_{(2k-1,2n-1,2m-1)})$

Hermite interpolation polynomials, as opposed to Lagrange polynomials, for which the expansion coefficients are function values and their derivatives at the nodes [14]. The additional derivative continuities required in this case substantially increase the accuracy of the eigenvalues. The global envelope function is constructed by summing contributions from all elements and ensuring the function value and its derivatives are continuous across the element. Further details from a physical point of view may be seen in Ref. [14] and we refrain from reporting more details of the method here. Since the finite-element approach may be viewed as the discretization of the action integral, we define the action from which Eq. (1) is derivable to be

$$\mathcal{A}/T = \int_V d^3r\ \psi^*\left[\overleftarrow{\partial}\cdot\frac{\hbar^2}{2m^*}\overrightarrow{\partial}+V(x,y,z)-E\right]\psi. \quad (3)$$

We here solve the time-independent problem so that the time integral over the range $[0,T]$ in the action is simply T. Dirichlet boundary conditions are implemented at the periphery of the physical region. In Fig. 1, we show the convergence of the error in the eigenvalues of the ground and the first excited state for different interpolation polynomials. Clearly, the Hermite interpolations yield more accurate results than the typical Lagrange

TABLE IV. Conduction-electron energy levels in GaAs/$Ga_{0.63}Al_{0.37}As$ QDs, with $m_w^* = 0.0665m_0$ and $m_b^* = 0.0858m_0$. The typical simplification of using an infinite well to evaluate the energy levels is seen to be in significant error since the finite potential is not separable.

		Energy (meV)	
Quantum numbers	Irreducible representation	$V = 276$	$V = \infty$
(1,1,1)	$1A_{1g}$	27.6398458	42.4094382
(1,1,2)	$1T_{1u}$	55.1963195	84.8188763
(1,2,1)		55.1963195	84.8188764
(2,1,1)		55.1963195	84.8188766
(1,2,2)	$1T_{2g}$	82.5703718	127.2283147
(2,1,2)		82.5703718	127.2283147
(2,2,1)		82.5703718	127.2283147
(1,1,3) + (1,3,1) + (3,1,1)	$1A_{1g}$	100.9570475	155.5012738
−(1,1,3) + 2(1,3,1) − (3,1,1)	$1E_g$	101.0083349	155.5012739
2(1,1,3) − (1,3,1) − (3,1,1)		101.0083349	155.5012739
(2,2,2)	$1A_{2u}$	109.7512732	169.6377529
(2,3,1) − (2,1,3)	$1T_{2u}$	128.0064988	197.9107120
(3,2,1) − (1,2,3)		128.0064988	197.9107121
(1,3,2) − (3,1,2)		128.0064988	197.9107121
(2,3,1) + (2,1,3)	$1T_{1u}$	128.0462602	197.9107121
(3,2,1) + (1,2,3)		128.0462602	197.9107121
(1,3,2) + (3,1,2)		128.0462602	197.9107121
(1,2,4) − (1,4,2)	$1T_{2g}$	190.8111029	296.8660777
(2,1,4) − (4,1,2)		190.8111029	296.8660777
(2,4,1) − (4,2,1)		190.8111029	296.8660777
(1,2,4) + (1,4,2)	$1T_{1g}$	191.3269094	296.8660777
(2,1,4) + (4,1,2)		191.3269094	296.8660777
(2,4,1) + (4,2,1)		191.3269094	296.8660778
(2,2,4) + (2,4,2) + (4,2,2)	$1A_{2u}$	216.6050003	339.2755159
−(2,2,4) + 2(2,4,2) − (4,2,2)	$1E_u$	217.5244549	339.2755160
2(2,2,4) − (2,4,2) − (4,2,2)		217.5244549	339.2755160

interpolation polynomials. In the case of finite barriers, there is a discontinuity in the potential and effective mass of the charge carriers at the interface between materials. Traditionally, while using Hermite finite elements, the continuity of the effective mass derivatives is ensured by patching the corresponding row vectors [5]. But this is a computationally expensive and slow process, especially in a parallel computing environment in 3D. We tackle this problem by representing the step function by a Fermi function. Thus the effective mass is given by

$$m^*(x,y,z) = m_b^* - \frac{m_b^* - m_w^*}{\left\{1+\exp\left[\frac{(x+\frac{a}{2})(x-\frac{a}{2})}{\delta^2}\right]\right\}\left\{1+\exp\left[\frac{(y+\frac{b}{2})(y-\frac{b}{2})}{\delta^2}\right]\right\}\left\{1+\exp\left[\frac{(z+\frac{c}{2})(z-\frac{c}{2})}{\delta^2}\right]\right\}}. \quad (4)$$

Similarly, the confining potential is defined by

$$V(x,y,z) = V_0\left(1 - \left\{1+\exp\left[\frac{(x+\frac{a}{2})(x-\frac{a}{2})}{\delta^2}\right]\right\}^{-1}\left\{1+\exp\left[\frac{(y+\frac{b}{2})(y-\frac{b}{2})}{\delta^2}\right]\right\}^{-1}\left\{1+\exp\left[\frac{(z+\frac{c}{2})(z-\frac{c}{2})}{\delta^2}\right]\right\}^{-1}\right). \quad (5)$$

Here, δ is the smoothing parameter or the "temperature" in the Fermi function, which controls the smoothing of the interfaces. By systemically decreasing the parameter δ, we mimic the finite barrier potential with a discontinuity. The most important benefit of this smoothing is that the properties of the function are the same on either side of the interface at any energy so that there are no jump conditions to implement in the calculations. We have verified this and the accuracy obtained in several test calculations. We note that the Fermi-function smoothing may be argued as a more physical material interface, though here we employ it for its simplicity in implementation for computation with the Hermite interpolation polynomials.

TABLE V. Light-hole energy levels in GaAs/$Ga_{0.63}Al_{0.37}As$ QDs, with $m_w^* = 0.0905m_0$ and $m_b^* = 0.1107m_0$. The typical simplification of using an infinite well to evaluate the energy levels is seen to be in significant error since the finite potential is not separable.

		Energy (meV)	
Quantum numbers	Irreducible representation	$V = 184$	$V = \infty$
(1,1,1)	$1A_{1g}$	20.2151693	31.1627363
(1,1,2)		40.3461623	62.3254726
(1,2,1)	$1T_{1u}$	40.3461623	62.3254727
(2,1,1)		40.3461623	62.3254728
(1,2,2)		60.3422579	93.4882091
(2,1,2)	$1T_{2g}$	60.3422579	93.4882091
(2,2,1)		60.3422579	93.4882091
(1,1,3) + (1,3,1) + (3,1,1)	$1A_{1g}$	73.6604738	114.2633670
−(1,1,3) + 2(1,3,1) − (3,1,1)	$1E_g$	73.7321914	114.2633670
2(1,1,3) − (1,3,1) − (3,1,1)		73.7321914	114.2633670
(2,2,2)	$1A_{2u}$	80.1946351	124.6509455
(2,3,1) − (2,1,3)		93.4188421	145.4261033
(3,2,1) − (1,2,3)	$1T_{2u}$	93.4188421	145.4261033
(1,3,2) − (3,1,2)		93.4188421	145.4261033
(2,3,1) + (2,1,3)		93.4736301	145.4261034
(3,2,1) + (1,2,3)	$1T_{1u}$	93.4736301	145.4261034
(1,3,2) + (3,1,2)		93.4736301	145.4261034
(1,2,4) − (1,4,2)		138.6920158	218.1391620
(2,1,4) − (4,1,2)	$1T_{2g}$	138.6920158	218.1391620
(2,4,1) − (4,2,1)		138.6920158	218.1391620
(1,2,4) + (1,4,2)		139.3460826	218.1391621
(2,1,4) + (4,1,2)	$1T_{1g}$	139.3460826	218.1391621
(2,4,1) + (4,2,1)		139.3460826	218.1391621
(2,2,4) + (2,4,2) + (4,2,2)	$1A_{2u}$	157.2405642	249.3018984
−(2,2,4) + 2(2,4,2) − (4,2,2)	$1E_u$	158.4166740	249.3018985
2(2,2,4) − (2,4,2) − (4,2,2)		158.4166740	249.3018985

Variation of the discretized action in Eq. (3) leads to a generalized eigenvalue matrix equation of the form $Av = EBv$, where A and B are sparse matrices of dimension equal to the total DoF and v is the eigenvector corresponding to the eigenvalue E. We solve this equation within a parallel computing environment [15–18]. We use the Krylov-Schur algorithm as implemented in SLEPc [19]. Here, we employ a spectral transformation by a shift-invert operator. The solver works with an equation of the form $(A - \lambda B)^{-1}Bv = \theta v$, where λ is the shift parameter. Energy eigenvalues are computed internally from the relation $E = \lambda + 1/\theta$. This procedure augments the convergence of eigenvalues near λ since the eigenvalues θ of the shift-invert operator are largest in magnitude for those energies in the vicinity of λ [16]. In the case of linear Lagrange interpolation polynomials, with 50 processors, matrices of dimensions 27000×27000 are assembled in 0.6 minutes and diagonalized in 2.9 minutes. On the other hand, using the quintic Hermite interpolation polynomials, with the same number of processors, matrices of the same dimensions are assembled in 70.0 minutes and diagonalized in 10.2 minutes. We pay the price for having to go through a larger number of loops while using the Hermite interpolation polynomials. This increase in time can be reduced by optimizing the number of processors used for the calculation.

The matrix bandwidth is defined as the sum of sub- and supradiagonal arrays together with the main diagonal. For a total of 27000 DoF, the linear Lagrange polynomials

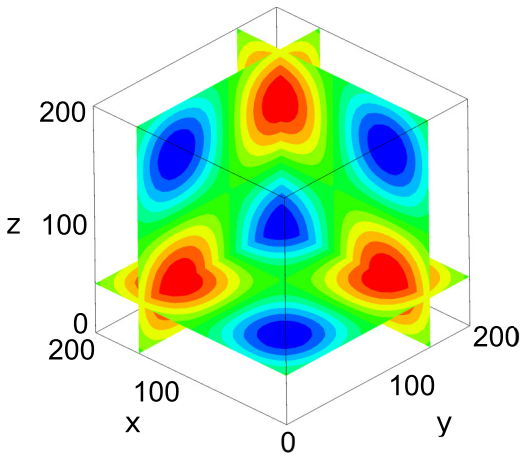

FIG. 3. Wave function for the (2,2,2) state of the cubic QD which is in the representation A_{2u}. Notice that the wave function is odd with respect to inversion about the center. Darker regions correspond to wave-function valleys (blue) and peaks (red), and lighter regions (green) correspond to values close to zero.

TABLE VI. Heavy-hole energy levels in GaAs/$Ga_{0.63}Al_{0.37}As$ QDs, with $m_w^* = 0.3774m_0$ and $m_b^* = 0.3865m_0$. The typical simplification of using an infinite well to evaluate the energy levels is seen to be in significant error since the finite potential is not separable.

Quantum numbers	Irreducible representation	Energy (meV)	
		$V = 184$	$V = \infty$
(1,1,1)	$1A_{1g}$	5.6339074	7.4727812
(1,1,2)	$1T_{1u}$	11.2717888	14.9455624
(1,2,1)		11.2717888	14.9455624
(2,1,1)		11.2717888	14.9455625
(1,2,2)	$1T_{2g}$	16.9084279	22.4183437
(2,1,2)		16.9084279	22.4183437
(2,2,1)		16.9084279	22.4183437
(1,1,3) + (1,3,1) + (3,1,1)	$1A_{1g}$	20.6978832	27.4001979
−(1,1,3) + 2(1,3,1) − (3,1,1)	$1E_g$	20.7001304	27.4001979
2(1,1,3) − (1,3,1) − (3,1,1)		20.7001304	27.4001979
(2,2,2)	$1A_{2u}$	22.5438146	29.8911249
(2,3,1) − (2,1,3)	$1T_{2u}$	26.3330823	34.8729792
(3,2,1) − (1,2,3)		26.3330823	34.8729792
(1,3,2) − (3,1,2)		26.3330823	34.8729792
(2,3,1) + (2,1,3)	$1T_{1u}$	26.3345962	34.8729792
(3,2,1) + (1,2,3)		26.3345962	34.8729792
(1,3,2) + (3,1,2)		26.3345962	34.8729792
(1,2,4) − (1,4,2)	$1T_{2g}$	39.6765282	52.3094705
(2,1,4) − (4,1,2)		39.6765282	52.3094705
(2,4,1) − (4,2,1)		39.6765282	52.3094705
(1,2,4) + (1,4,2)	$1T_{1g}$	39.6883222	52.3094705
(2,1,4) + (4,1,2)		39.6883222	52.3094705
(2,4,1) + (4,2,1)		39.6883222	52.3094705
(2,2,4) + (2,4,2) + (4,2,2)	$1A_{2u}$	45.3002293	59.7822517
−(2,2,4) + 2(2,4,2) − (4,2,2)	$1E_u$	45.3181042	59.7822517
2(2,2,4) − (2,4,2) − (4,2,2)		45.3181042	59.7822517
(1,3,5) − (1,5,3) + (3,5,1) − (3,1,5) + (5,1,3) − (5,3,1)	$1A_{1g}$	67.0254522	87.1824696
(1,3,5) + (1,5,3) + (3,5,1) + (3,1,5) + (5,1,3) + (5,3,1)	$1A_{2g}$	67.0857917	87.1824696
2(1,3,5) − (3,5,1) − (5,1,3)	$2E_g$	67.0311478	87.1824696
2(3,5,1) − (5,1,3) − (1,3,5)		67.0311478	87.1824696
2(3,1,5) − (1,5,3) − (5,3,1)		67.0805808	87.1824696
2(1,5,3) − (3,1,5) − (5,3,1)		67.0805808	87.1824696

utilize a bandwidth of 53987, while the quintic Hermite interpolation polynomials occupy a comparable bandwidth of 53903. The occupancy of a matrix is defined as the percentage of nonzero entries in the matrix. While going from the linear Lagrange to quintic Hermite polynomials, there is only a nominal increase in the matrix occupancy from 0.214% to 0.929% for the B matrix and 0.06% to 0.928% for the A matrix. The increase in computational time with the Hermite interpolation calculations is compensated considerably by the higher accuracy delivered, as seen in Fig. 1.

III. DEGENERACY AND THE POINT-GROUP SYMMETRY

Degeneracies in the energy spectrum arise from symmetries associated with the geometry. They are equal to the dimensions of the irreducible representations of the corresponding symmetry group [20,21]. Any other additional degeneracy which cannot be explained by the obvious geometrical symmetry of the system is labeled as accidental degeneracy. Accidental degeneracies are rendered normal by identifying the hidden covering group.

We know that for a three-dimensional infinite barrier cubic QD of length L, the energy eigenvalues are given by

$$E(n_1,n_2,n_3) = \left(\frac{\hbar^2\pi^2}{2m^*L^2}\right)\left(n_1^2 + n_2^2 + n_3^2\right), \qquad (6)$$

where $n_1,n_2,n_3 \in \mathbb{N}$. Energy eigenvalues reside on the first octant of the number sphere. From Fig. 2(a), we see that the degree of degeneracy increases with increase in energy; within the exploration done by us, it reaches fairly large values.

In the continuum limit, the density of states is equal to the area of positive octant in the number sphere which goes as $\sqrt{E}$.

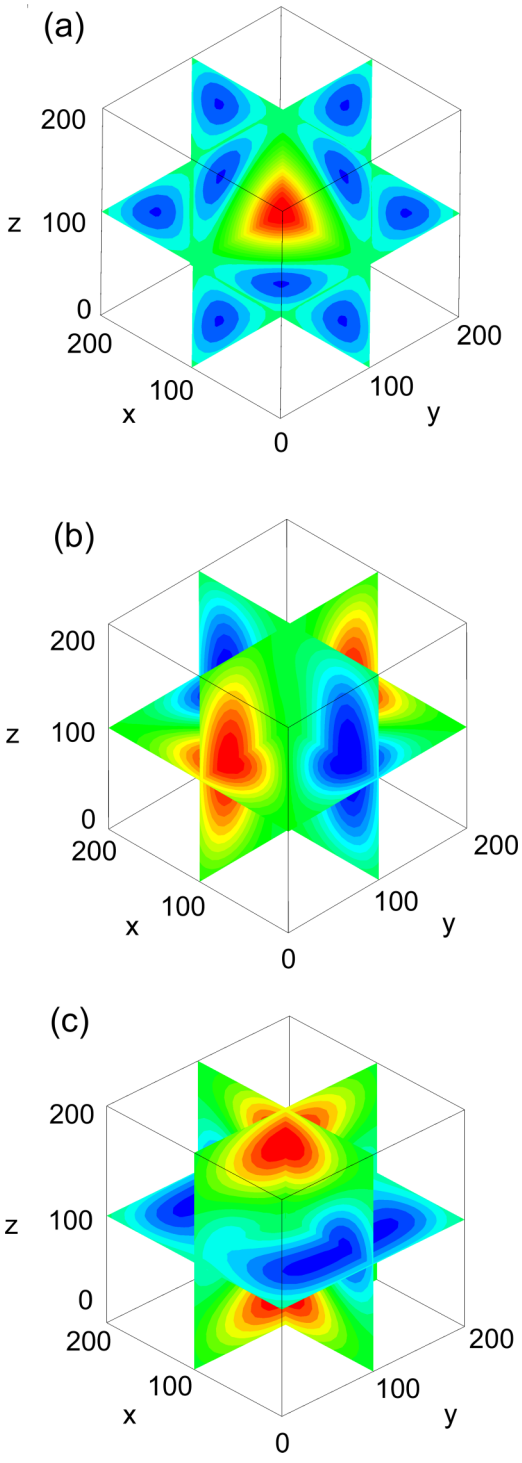

FIG. 4. Wave functions for (a) the state $(1,1,3)+(1,3,1)+(3,1,1)$ belonging to the representation A_{1g}, which has full O_h symmetry, and (b) the state $-(1,1,3)-(1,3,1)+2(3,1,1)$ and (c) the state $-(1,1,3)+2(1,3,1)+(3,1,1)$, which are in the representation E_g of the group O_h. These two states are related by a C_4 rotation about the x axis. Darker regions correspond to wave-function valleys (blue) and peaks (red), and lighter regions (green) correspond to values close to zero.

This semiclassical evaluation overestimates the true density [see Fig. 2(b)] for low energies. However, the theoretical continuum approximation is in excellent agreement already for intermediate energies. The averaging procedure to obtain the density of degenerate states is done as follows. For this problem, the states lie in the positive quadrant of the number space. The degeneracy is sorted by distributing the n values into bins of thickness $dn^2 = 2ndn$, where $dn = 1$ or any suitable small number. The degeneracies of all states in this shell are added, and divided by the size of the bin which equals dn^2. The density of states versus energy is directly obtained by noting that $n^2 \propto E$. The analytical curve plotted in Fig. 2 is $n\pi/4$.

Note that there are two kinds of degeneracies present. The first kind is due to the exchange of quantum numbers that are listed in Table I. The second kind is less transparent, occurring when the following relation is satisfied:

$$n_1^2 + n_2^2 + n_3^2 = m_1^2 + m_2^2 + m_3^2, \tag{7}$$

with $n_i \neq m_j$, for $i,j = 1,2,3$. Cubic QDs have geometrical octahedral symmetry (O_h). The character table for the point group O_h is given in Ref. [21]. We see that O_h has only one-, two-, and three-dimensional representations. The energy spectrum with infinite barrier approximation, on the other hand, displays degeneracies of higher order (see Fig. 2). The accidental degeneracies due to the permutation of quantum numbers can be accounted for by finding the covering group, which is a semidirect product of the geometrical symmetry group O_h and a two-dimensional compact continuous group [22]. The dynamical operators $(\partial_x^2 - \partial_y^2)$ and $(2\partial_z^2 - \partial_x^2 - \partial_y^2)$ connect the accidental degeneracies generated by the permutation of the quantum numbers [23].

For finite barriers, the potential is nonseparable and the accidental degeneracy present in the infinite barrier case is lifted. However, it suffices to use the infinite barrier quantum numbers for labeling the eigenstates. For the finite barrier, the states can be labeled with quantum numbers (n_1,n_2,n_3), as products of sine functions. We require degenerate symmetry-adapted linear combinations of wave functions to form the basis for their irreducible representations. We shall thus classify the wave functions into their corresponding irreducible representations under O_h. Our approach is similar to that of Ref. [23]. Let G be a group of the order of g and $\Gamma^{(i)}$ be an l_i-dimensional representation of G. For a group element R in G, its representation is given by an $l_i \times l_i$ square matrix $\Gamma^{(i)}(R)$. Then the projection operator [20] corresponding to $\Gamma^{(i)}$ is given by

$$\mathcal{P}^{(i)} = \frac{l_i}{g} \sum_R \chi^{(i)}(R) \cdot P_R, \tag{8}$$

where $\chi^{(i)}(R)$ is the character and P_R is the operator corresponding to the element R. The projection operator $\mathcal{P}^{(i)}$ projects out a function F onto a part $f^{(i)}$ belonging to the representation $\Gamma^{(i)}$. Let $\{\psi_i\}_{i=1}^n$ be a basis set of Hilbert space $\mathcal{H}$ which is in a representation Γ. In general, Γ is a reducible representation of the symmetry group of $\mathcal{H}$. Let F be a general function in $\mathcal{H}$. Consider

$$\mathcal{P}^{(i)} F = f^{(i)} = \sum_{j=1}^{n} c_j^{(i)} \psi_j, \tag{9}$$

where the coefficients are given by

$$c_j^{(i)} = \int_V d^3r \; \psi_j^\dagger (\mathcal{P}^{(i)} F). \tag{10}$$

TABLE VII. Lowering of symmetry and splitting of degeneracy in the presence of 1 and 20 kV/cm electric fields, in the conduction and valence bands.

		Energy (meV)					
		Conduction electron		Light hole		Heavy hole	
O_h	C_2	$E = 1$ kV/cm	$E = 20$ kV/cm	$E = 1$ kV/cm	$E = 20$ kV/cm	$E = 1$ kV/cm	$E = 20$ kV/cm
A_{1g}	A_1	30.6325979	84.8862722	23.2051825	76.5630495	8.6034888	33.1401019
T_{1u}	E	58.1889961	112.4161376	43.3360671	96.6588056	14.2413581	38.7771958
		58.1889961	112.4161376	43.3360671	96.6588056	14.2413581	38.7771958
	A_1	58.1984405	115.9042693	43.3490347	101.1657821	14.2809973	41.6810315
T_{2g}	B_2	85.5629672	139.7615889	63.3320451	116.6166870	19.8779849	44.4130404
	E	85.5725060	143.2800955	63.3451447	121.1595178	19.9176394	47.3175751
		85.5725060	143.2800955	63.3451447	121.1595178	19.9176394	47.3175751
A_{1g}	A_1	103.9521350	158.1420019	76.6536618	129.9254484	23.6681493	48.2026497
E_g	A_1	104.0008677	158.1774663	76.7218842	129.9759093	23.6696783	48.2041586
	B_1	104.0069928	161.4718371	76.7302898	134.3320494	23.7051839	51.2423583
A_{2u}	B_2	112.7534207	170.4624429	83.1975354	141.0083372	25.5530291	52.9528650
T_{2u}	E	131.0028179	185.1617222	96.4137044	149.6430428	29.3033586	53.8370547
		131.0028179	185.1617222	96.4137044	149.6430428	29.3033586	53.8370547
	B_1	131.0086546	188.7178983	96.4217482	154.2270192	29.3422989	56.7420587
T_{1u}	E	131.0435892	188.5047413	96.4698984	154.0608113	29.3396284	56.8769143
		131.0435892	188.5047413	96.4698984	154.0608113	29.3396284	56.8769143
	A_1	131.0484164	188.7579213	96.4765378	154.2830307	29.3438128	56.7435743
T_{2g}	B_2	193.8032019	247.8271711	141.6809651	194.6891392	42.6460290	67.1775006
	E	193.8123939	251.1427793	141.6935107	198.9264968	42.6825840	70.0747385
		193.8123939	251.1427793	141.6935107	198.9264968	42.6825840	70.0747385
T_{1g}	A_2	194.3190594	248.3613205	142.3351739	195.3932421	42.6578243	67.1893760
	E	194.3283039	251.8995372	142.3478390	199.9665636	42.6954763	70.0932419
		194.3283039	251.8995372	142.3478390	199.9665636	42.6954763	70.0932419
A_{2u}	B_2	219.6064854	276.9942886	160.2421359	212.1353850	48.3073497	75.7013152
E_u	A_2	220.5255529	277.9842400	161.4179343	216.6605758	48.3241968	75.7200343
	B_2	220.5266410	278.2286577	161.4195642	218.4187036	48.3273319	75.7267123

Similarly, for a basis function ψ_k, we write

$$c_{jk}^{(i)} = \int_V d^3r \; \psi_j^\dagger (\mathcal{P}^{(i)} \psi_k). \tag{11}$$

If the coefficient is nonzero, the wave function ψ_k has a component in the ith representation and ψ_j is a partner. Once we determine all coefficients, from Eq. (9) we obtain a new basis function $f^{(i)}$ which is exclusively in the ith representation. Using this procedure, we list out all basis functions and irreducible representations for different combinations of quantum numbers in Tables II and III. These new functions that are listed in the third column of Tables II and III are a more natural choice for the basis set as they are compatible with the symmetry of irreducible representations. For instance, a basis function for A_{1g}, the symmetric irreducible representation, should have total symmetry of the group under consideration.

IV. RESULTS AND DISCUSSIONS

We have used the infinite-barrier quantum dot to determine the degeneracy of levels and how well the continuum approximation reproduces the discrete degeneracies. More importantly, we have determined the level of accuracy achieved in our numerical calculations with the infinite-barrier QD for which the eigenvalues are known analytically. We expect that the eigenvalues obtained with a finite well will have almost the same level of accuracy given that the finite-well QD calculations are not altering the input numerical values in any significant way. In Tables IV–VI, we list the calculated eigenvalues for conduction electrons, light holes, and heavy holes in $GaAs/Ga_{0.3}Al_{0.37}As$ cubic QDs of dimensions $200\times200\times200$ Å.

We represent each eigenstate by a symmetry-adapted linear combination of quantum numbers (n_1,n_2,n_3) associated with the infinite well. For comparison, we include energy values obtained using the infinite-barrier approximation. Note that all of the energy levels are lowered from the values obtained with infinite barriers. Additional accidental degeneracies observed in the case of an infinite barrier are lifted. Clearly, the infinite-barrier approximation is invalid in this case. States

TABLE VIII. Lowering of symmetry and splitting of degeneracy in the presence of 1 and 5 T magnetic fields, in the conduction and valence bands.

		Energy (meV)					
		Conduction electron		Light hole		Heavy hole	
O_h	C_2	$E = 1\,\mathrm{kV/cm}$	$E = 20\,\mathrm{kV/cm}$	$E = 1\,\mathrm{kV/cm}$	$E = 20\,\mathrm{kV/cm}$	$E = 1\,\mathrm{kV/cm}$	$E = 20\,\mathrm{kV/cm}$
A_{1g}	A	26.4932919	-4.8840368	19.3877141	-3.6434403	5.4796057	0.2583186
T_{1u}	A	53.2169808	20.1339720	38.9058124	14.6228892	10.9697672	5.3887369
	$2B$	54.0533223	22.7498785	39.5211104	16.5374219	11.1174958	5.8963006
		54.8778163	28.5790951	40.1276664	20.8389901	11.2641614	6.8571786
T_{2g}	A	80.5974595	47.6065125	58.9062332	34.6836094	16.6064203	11.0255338
	$2B$	81.2683771	50.2308227	59.3984048	36.6027622	16.7298280	11.4770314
		82.2530234	56.0301517	60.1245542	40.8857484	16.9008023	12.4939400
A_{1g}	A	99.8112184	68.6822477	72.8334077	49.9887205	20.5430893	15.3240647
E_g	$2A$	99.8679240	69.8135450	72.9084944	50.8177405	20.5456429	15.5922676
		100.0224376	73.9183335	73.0238855	53.8911239	20.5715086	16.1463884
A_{2u}	A	108.4532026	77.5113507	79.2532896	56.5196614	22.3652178	17.1125332
T_{2u}	A	125.2321307	90.1747291	91.4051820	65.6532810	25.8860778	19.8888774
	$2B$	126.0649696	93.2403029	92.0177721	67.9066859	26.0318545	20.4512219
		126.8611243	96.9336933	92.5916335	70.6069265	26.1780867	21.2266782
T_{1u}	A	127.0645735	101.0549274	92.7682625	73.6991187	26.2059804	21.7809729
	$2B$	127.7112690	101.6253733	93.2303424	74.0832072	26.3262177	21.9195661
		128.4123280	104.9692553	93.7436684	76.4960686	26.4558632	22.6043168
T_{2g}	A	189.0605140	156.5853517	137.4743812	113.6789607	39.3802735	33.8002305
	$2B$	189.6253297	160.8458778	137.8324884	116.6043714	39.5216559	34.7197963
		189.9392687	161.5775929	138.1083802	117.3658824	39.5322679	34.8313813
T_{1g}	A	190.0764546	161.7920168	138.3869186	117.7610849	39.5658830	34.9417166
	$2B$	190.5608435	162.9376707	138.8011010	118.3459505	39.6026739	35.1853338
		190.8418389	164.3101030	138.9635594	119.4525947	39.6751075	35.2686268
A_{2u}	A	215.3905447	185.3730561	156.3601221	134.4008619	45.1302652	39.8812443
E_u	$2A$	216.2796612	187.1525114	157.5121694	135.8308242	45.1545845	40.3494853
		216.7630847	193.1348911	157.8743777	139.9227037	45.2324644	41.7345863

with a symmetric combination of quantum numbers are more bound than others. For example, states corresponding to A_{1g} and A_{2u} have lower energies than that of E_g and E_u, respectively. As expected, we see only one-, two-, and three-level degeneracies. States that were six-level degenerate in the case of infinite-barrier approximation are split into two triplet states for (two even and one odd) or (two odd and one even) combinations of quantum numbers. For all three different odd or even combinations, states will split into two singlets and two doublets as expected (see Table III). In Fig. 3, we have shown the wave function for the (2,2,2) state projected along three perpendicular planes. We see that the wave function is odd with respect to the inversion center, since it is in the representation A_{2u}. The wave functions of (1,1,3), (1,3,1), and (3,1,1) states split into a singlet and a degenerate doublet. In Fig. 4(a), we see that the singlet, which is in the A_{1g} representation, has the complete O_h symmetry. The doublets belonging to the E_g representation are related by a proper C_4 rotation around the x axis [see Figs. 4(b) and 4(c)].

We can induce level splitting by having an additional perturbation. Thus the symmetry is reduced to one of the subgroup of O_h. The original Hamiltonian H_0 belongs to the irreducible representation A_1 of O_h. The additional perturbation H' may not have the complete O_h symmetry. We determine the new symmetry by finding the subgroup G of maximum dimension in which all the terms of H' form a basis for the irreducible representation A_1 in G. For example, consider an external constant electric field $H' = -eE_0z$ applied to a cubic QD. We note that C_{4v} is the subgroup of maximum dimension in which z is a basis of the representation A_1. Hence, O_h symmetry is reduced to C_{4v} symmetry. We decompose all irreducible representations of O_h through direct products of

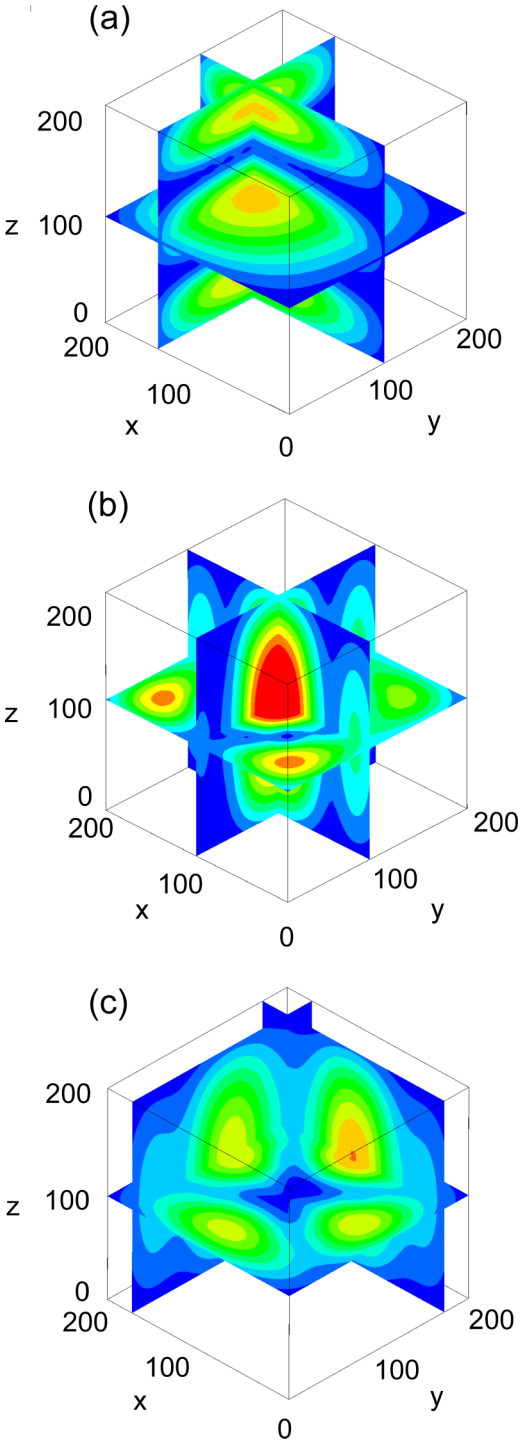

FIG. 5. Probability densities for the states (1,1,3), (1,3,1), and (3,1,1) of the cubic QD in a 5 T magnetic field along the $\hat{z}$ axis. The magnetic field splits all states into singlets whose symmetry is reduced to the group C_2. Darker regions correspond to wave-function nodes (blue) and antinodes (red), and lighter regions correspond to values in between.

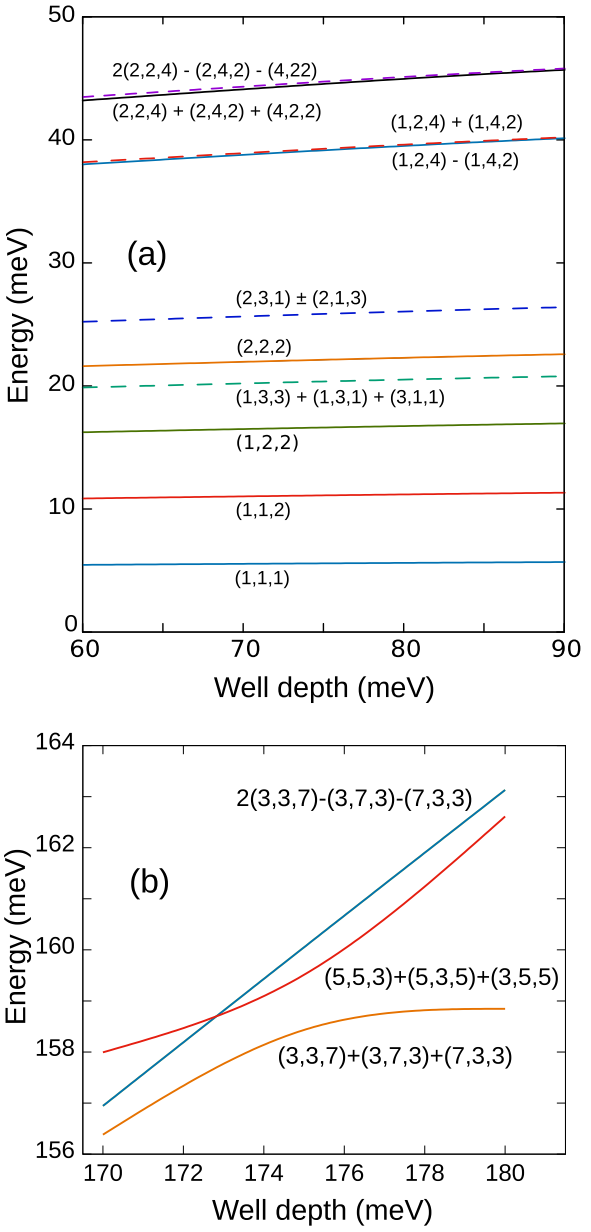

FIG. 6. The dependence of heavy-hole energy levels on the barrier height in a 200×200×200 Å cubic QD for (a) the first 10 energy levels and (b) a selected few higher states in which level crossing is observed.

irreducible representations of C_{4v} [24]. In Table VII, we list out numerically obtained eigenvalues for the cubic QD in an electric field. Level splitting is in accordance with group theoretical predictions. For an applied magnetic field $\boldsymbol{B}$ and corresponding vector potential $\boldsymbol{A}$, the perturbing Hamiltonian is given by

$$H' = \frac{e}{m}\boldsymbol{A}.\boldsymbol{p} + \frac{e^2}{2m}|\boldsymbol{A}|^2 - \boldsymbol{\mu}\cdot\boldsymbol{B}, \tag{12}$$

where $\boldsymbol{\mu} = -(e/m)\boldsymbol{S}$ and $\boldsymbol{S}$ is the spin angular momentum. For a constant field $\boldsymbol{B} = B_0\hat{z}$, within the Landau gauge, the vector potential is given by $\boldsymbol{A} = B_0\, x\, \hat{y}$. Hence, H' has terms that transform as xy and x^2. The spin-orbit-coupling term contributes only up to a constant value and it has the complete O_h symmetry. By inspection, we see that only the subgroup C_2 has all these terms belonging to its trivial representation A. We verify from Table VIII that all energy levels are split into nondegenerate states as the group C_2 has only one-dimensional representations. In Fig. 5, we see that in an applied magnetic

field, the probability distribution of electrons retains only C_2 symmetry.

Finally, we study the dependence of level splitting on barrier height for heavy holes in GaAs/$Ga_{(1-x)}Al_xAs$ cubic QDs of dimensions 200×200×200 Å. As expected, level splitting between energy levels decreases [see Fig. 6(a)] and approaches that of an infinite barrier in the limit $V \rightarrow \infty$. In some cases, there is a level crossing between states of different quantum numbers. In Fig. 6(b), we see that energy of the state (5,5,3) + (5,3,5) + (3,5,5) reduces below the energy of state 2(3,3,7) − (3,7,3) − (7,3,3) for well depth $\geqslant$ 173 meV. Hence, even the ordering of energy levels is a function of well depth.

V. CONCLUSIONS

We have developed a formalism based on FEA which provides accurate energy spectra and symmetry-adapted wave functions for a cubic quantum dot. Such accuracy is pivotal to study linear and nonlinear optical, electrical, and magnetic properties of a quantum dot. It is clear that the infinite-barrier approximation leads to serious errors and additional (accidental) degeneracies. The group-representation theory provides a robust method to predict degeneracies in the energy spectrum and symmetry-adapted wave functions by just knowing the symmetries of the associated Hamiltonian. We have derived a coefficient formula which determines the basis for all irreducible representations of the symmetry group. Our method is general and can be easily extended to find the energy spectrum for a quantum dot of any shape and size.

In layered semiconductor structures, FEA allows us to treat the issue of self-consistently solving the Schrödinger-Poisson equations to derive the changes in the band-edge profile for arbitrary doping with impurities in arbitrary layers [25]. The ionized impurities are held in place while the carriers that are freed are distributed in a self-consistent manner in the heterostructure. In modulation-doped cubic QDs, the impurity concentration, typically in the barrier, leads to a self-consistent reconfiguration of the band edges. Lee *et al.* [26] proposed a numerical method to obtain self-consistent solutions to the Schrödinger-Poisson equations in cubic QDs with finite barriers. However, their expansion of wave functions in terms of separable global orthogonal periodic functions are expected to give inaccurate results since the finite potential itself is not separable. Extension of our method should provide a highly reliable solution, as we can systematically increase the accuracy through mesh-size refinement (h-refinement) or by the use of higher-order interpolation polynomials (p-refinement) for convergence within the FEA. Such freedom is lost when using global basis functions.

In II-VI semiconductors, the inclusion of a dilute distribution of magnetic ions such as Mn leads to a dramatic change in the magnetic properties of the material. In CdMnTe, for example, the acceptor bound magnetic polarons are formed by the presence of the magnetic ions within the Bohr radius of the impurity state, which leads to a large change in the binding energy of the acceptor. The hydrogenic acceptor state has a magnetic exchange contribution that leads to a highly nonlinear Schrödinger equation. This is readily solved to obtain the new binding energy of the bound magnetic polaron [27]. A similar doping with Mn of a GaAs quantum well has the Mn entering the crystal as a *p*-type impurity, and releasing a very large number of holes in the well even for small stoichiometric concentrations. This has been calculated by us using FEA [28]. We note that doping dilutely with Mn ions in the GaAs QDs again leads to a release of a large number of holes in the QD region. Such a structure also requires a self-consistent solution.

The optical second-order susceptibility in asymmetric quantum wells has been well studied [29], and the third-order optical susceptibility in checkerboard superlattices of quantum wires was investigated by us earlier [30]. In the literature, typically for QDs, the second- and third-order nonlinear optical susceptibilities are obtained using the infinite-barrier approximation [31,32]. It will be of interest to examine the influence of finite barriers in the presence of external electric and magnetic fields, as delineated in this paper, in view of the more accurate solutions we obtain within our framework.

Our method can be adapted to study both spatial and spin entanglement of two or more electrons in double quantum dots. We require special techniques to evaluate computationally demanding Coulomb integrals. These calculations will be presented elsewhere.

Lastly, we note that our method is well suited to study correlation and quantum confinement of excitons in QDs. FEA can be easily extended to solve the Schödinger equation in six dimensions.

ACKNOWLEDGMENTS

We thank the Center for Computational NanoScience (CCNS) at Worcester Polytechnic Institute for the computational resources used for these calculations. S.P. wishes to thank Worcester Polytechnic Institute for support through the summer undergraduate research award.

[1] J. J. Sakurai, *Modern Quantum Mechanics* (Addison-Wesley, Reading, MA, 1994).
[2] W. Pauli, Z. Phys. **36**, 336 (1926).
[3] V. Fock, Z. Phys. **98**, 145 (1935).
[4] A. O. Barut and H. Kleinert, Phys. Rev. **161**, 1464 (1967); H. Kleinert, Fortschr. Phys. **16**, 1 (1968).
[5] J. Shertzer and L. R. Ram-Mohan, Phys. Rev. B **41**, 9994 (1990).
[6] F. Leyvarz, A. Frank, R. Lemus, and M. V. Andrez, Am. J. Phys. **65**, 1087 (1997).
[7] F. Reif, *Fundamentals of Statistical and Thermal Physics* (McGraw-Hill, New York, 1965).
[8] S. L. Chuang, *Physics of Optoelectronic Devices* (Wiley, New York, 1995).
[9] M. Balkanski and R. F. Wallis, *Semiconductor Physics and Applications* (Oxford University Press, New York, 2000).
[10] P. Harrison and A. Valavanis, *Quantum Wires and Dots, in Quantum Wells, Wires and Dots: Theoretical and Computational Physics of Semiconductor Nanostructures*, 4th ed. (Wiley, Chichester, UK, 2016).

[11] G. Bastard, Phys. Rev. B **24**, 5693 (1981); **25**, 7584 (1982); also see L. R. Ram-Mohan, K. H. Yoo, and R. L. Aggarwal, *ibid.* **38**, 6151 (1988), and references therein.

[12] D. J. BenDaniel and C. B. Duke, Phys. Rev. **152**, 683 (1966); In the multiband context, the probability current continuity condition can be obtained directly from the Lagrangian density, as in L. R. Ram-Mohan, J. R. Meyer, and I. Vurgaftman, J. Microelectron. **30**, 1031 (1999); L. R. Ram-Mohan, in *Proceedings of the 31st International Symposium Compound Semiconductors*, edited by Y.-S. Kwon, T. Yao, K.-H. Yoo, H. Hasegawa, and J. C. Woo, AIP Conf. Ser. 184 (IoP, Bristol, UK, 2005), pp. 1–8; L. R. Ram-Mohan and K. H. Yoo, J. Phys.: Condens. Matter **18**, R901 (2006).

[13] I. Vurgaftman, J. R. Meyer, and L. R. Ram-Mohan, J. Appl. Phys. **89**, 5815 (2001).

[14] L. R. Ram-Mohan, *Finite and Boundary Element Applications in Quantum Mechanics* (Oxford University Press, New York, 2002).

[15] S. Balay, S. Abhyankar, M. F. Adams, J. Brown, P. Brune, K. Buschelman, L. Dalcin, V. Eijkhout, W. D. Gropp, D. Kaushik, M. G. Knepley, D. A. May, L. Curfman McInnes, K. Rupp, P. Sanan, B. F. Smith, S. Zampini, H. Zhang, and H. Zhang, PETSc users manual, Tech. Rep. ANL-95/11 - Revision 3.8, Argonne National Laboratory (2017).

[16] V. Hernandez, J. E. Roman, and V. Vidal, ACM Trans. Math. Software **31**, 351 (2005).

[17] P. R. Amestoy, I. S. Duff, J.-Y. L'Excellent, and J. Koster, SIAM J. Matrix Anal. Appl. **23**, 15 (2006).

[18] X. S. Li and J. W. Demmel, ACM Trans. Math. Software **29**, 110 (2003).

[19] V. Hernandez, J. E. Roman, A. Tomas, and V. Vidal, *Krylov-schur Methods in SLEPc.* Tech. Rep. No. STR-7, Universitat Politécnica de Valéncia, 2009 (unpublished); also, see G. W. Stewart, SIAM J. Matrix Anal. Appl. **23**, 601 (2002).

[20] M. Tinkham, *Group Theory and Quantum Mechanics* (Dover, New York, 2003).

[21] M. S. Dresselhaus, G. Dresselhaus, and A. Jorio, *Group Theory: Application to the Physics of Condensed Matter* (Springer, Berlin, 2008).

[22] A. O. Hernandez-Castillo and R. Lemus, J. Phys. A: Math. Theor. **46**, 465201 (2013).

[23] F. M. Fernandez, arXiv:1310.5136.

[24] H. Bethe, Ann. Phys. **3**, 133 (1929).

[25] L. R. Ram-Mohan, K. H. Yoo, and J. Moussa, J. Appl. Phys. **95**, 3081 (2004).

[26] J. Lee, H. N. Spector, and W. C. Chou, Phys. Status Solidi B **242**, 2846 (2005).

[27] L. R. Ram-Mohan and P. A. Wolff, Phys. Rev. B **38**, 1330 (1988).

[28] S. T. Jang, K. H. Yoo, and L. R. Ram-Mohan, J. Korean Phys. Soc. **50**, 834 (2007).

[29] I. Vurgaftman, J. R. Meyer, and L. R. Ram-Mohan, IEEE J. Quantum Electron. **32**, 1334 (1996).

[30] L. R. Ram-Mohan and J. Shertzer, Appl. Phys. Lett. **57**, 282 (1990).

[31] S. Shao, K.-X. Guo, Z.-H. Zhang, N. Li, and C. Peng, Physica B **406**, 393 (2011).

[32] Z.-H. Zhang, K.-X. Guo, B. Chen, R.-Z. Wang, and M.-W. Kang, Superlattices Microstruct. **46**, 672 (2009).